Modelling oxygen effects on the in- and out-of-field radiosensitivity of cells exposed to intensity-modulated radiation fields

Yusuke Matsuya[1,5], Stephen J. McMahon[2], Karl Butterworth[2], Yoshie Yachi[3], Ryo Saga[4], Tatsuhiko Sato[1], Kevin M. Prise[2]

[1] *Nuclear Science and Engineering Center, Japan Atomic Energy Agency, Tokai, Japan*
[2] *Patrick G Johnston Centre for Cancer Research, Queen's University Belfast, Belfast, United Kingdom*
[3] *Graduate School of Health Sciences, Hokkaido University, Sapporo, Japan*
[4] *Graduate School of Health Sciences, Hirosaki University, Hirosaki, Japan*
[5] *Faculty of Health Sciences, Hokkaido University, Sapporo, Japan*
*Corresponding author: matsuya.yusuke@hs.hokudai.ac.jp (Yusuke Matsuya)

ABSTRACT

Objective: The delivery of intensity-modulated radiation fields has improved the conformity of dose to tumour targets during radiotherapy (RT). Previously, it has been shown that intercellular communication between cells positioned in- and outside of the radiation field impacts cellular radiosensitivity under hypoxic and normoxic conditions. However, the mechanism of intercellular communication in hypoxia remains to be fully understood. In this study, the cell-killing effects of intercellular communication in hypoxia were modelled in an effort to better understand the underlying mechanisms of response.

Approach: By irradiating a 50% area of the culture dish (half-field exposure), experimental dose-response curves for cell survival and residual DNA double-strand breaks (DSBs) were generated in prostate (DU145) and non-small cell lung cancer (H1299) cells. The oxygen enhancement ratio (OER) was determined from early DSB yields (corresponding to relative direct damage) and used to model the in- and out-of-field radiosensitivity.

Main results: The developed *integrated microdosimetric-kinetic (IMK) model* successfully predicted the experimental dose responses for survival and lethal lesions, and provides a mechanistic interpretation that the probability of hits for releasing cell-killing signals is dependent on oxygen. This experimental and modelling study also suggests that residual DSBs correspond to logarithmic survival fraction (meaning lethal lesions) for in- and out-of-field cells. Our data suggest that the OER value determined using uniform-field exposure can be applied to predict the in- and out-of-field radiosensitivity of cells following exposure to intensity modulated beams.

Significance: The developed IMK model facilitates a more precise understanding of intercellular signalling following exposure to intensity-modulated radiation fields.

Keywords: Hypoxia, biophysical model, cell survival, lethal damage, intercellular signaling.

1. Introduction

The efficacy of radiotherapy (RT) is dependent on biological factors that impact the process of cellular repair, redistribution, repopulation and reoxygenation (Wither 1975). Hypoxia

is a key factor that drives radioresistance (Garty *et al* 1953) and various strategies have been explored to selectively target hypoxic cells including oxygen-nicotinamide, bioreductive drugs (Laurence *et al* 1995, McKeown *et al* 2007) and fractionated treatment regimens (Sugano *et al* 2015) using intensity-modulated RT (IMRT) and volumetric modulated arc therapy (VMAT) that are the established clinical standard in advanced conformal RT (Kuperman *et al* 2008, McGary *et al* 2011). During the delivery of modulated RT techniques, the 3-dimensional dose distribution within target tumour volumes is highly heterogeneous at the cellular level and can induce intercellular signalling between irradiated and non-irradiated cells (Prise *et al* 2009, Butterworth *et al* 2011). This intercellular signalling can modulate the radiosensitivity of cells in- and out-of-field through protective (in-field) (Matsuya *et al* 2019 2022) and bystander effects (out-of-field) (Butterworth *et al* 2011, Trainor *et al* 2012, Ghita *et al* 2015). An improved understanding of the mechanisms of cellular response to intensity-modulated radiation fields could potentially lead to the further optimisation of treatments by maximising the probability of tumour control (TCP) and reducing the normal tissue complication probability (NTCP) (Bentzen *et al* 2009).

To investigate cellular radiosensitivity under intensity-modulated radiation fields, the oxygen enhancement ratio (OER), defined as the dose ratio between exposure in hypoxia and in air for the same biological endpoint (Hall *et al* 2010) has been evaluated *in vitro*. We have previously shown the impact of hypoxia on out-of-field cell survival after 4 or 8 Gy irradiation appeared to be independent of oxygen concentration (Thompson *et al* 2017). Further experimental studies have shown that hypoxia can have significant effects on out-of-field radiosensitivity that are dependent on the in-field dose. Also, the maximum level of cell killing for out-of-field cancer cells (i.e., DU145 and H1299) after irradiation with high in-field dose is known to be less dependent on oxygen (Matsuya *et al* 2021). Together, these data show that intercellular signalling in hypoxia can enhance out-of-field cell killing, however, responses under hypoxia remain to be fully characterised.

Radiobiological studies combined with modelling approaches are an effective approach towards better understanding the potential mechanisms of intercellular signalling (McMahon *et al* 2012, Sato *et al* 2018b, Scholz *et al* 2020, Matsuya *et al* 2018 2020a, Monini *et al* 2019). Amongst the various mechanistic models for predicting cell killing, the "integrated microdosimetric-kinetic model (IMK) model" explicitly considers DNA damage kinetics (Matsuya *et al* 2018), intercellular signalling (Matsuya *et al* 2019) and oxygen effects (Matsuya *et al* 2020a). Taking account of these features, further development of the *IMK model* is expected to enable us to mechanistically interpret the scenario of intercellular signalling in hypoxia.

In this study, we investigated intercellular signalling in hypoxia from the standpoint of IMK model development. Using a shielding technique where only 50% of the area of a cell culture dish is exposed (i.e., half-field exposure) (Trainor *et al* 2012), we generated experimental dose-response curves for cell survival and residual nuclear DNA damage for prostate cancer cells (DU145) and small cell lung cancer (H1299). Using a common OER value, we modelled the in-field and out-of-field radiosensitivities based on the oxygen-dependent hit probabilities of target

DNA and signal release elements. Throughout this study, we propose the dominant impact of intercellular signalling and a theoretical model useful for future predictions in radiation therapy.

2. Overview of Model Development

2-1. *Assumptions of Oxygen Effects in the IMK model*

The biological effects after half-field exposure are believed to be induced by DNA-targeted effects (Hall *et al* 2006) and intercellular signaling (Prise *et al* 2009). A schematic illustration of a half-field exposure setup is shown in Fig. 1(A), and the biological effects from the half-field exposure is illustrated in Fig 1(B). For the targeted effects, in the presence of O_2, the interaction between radiation and liquid water produces several types of free radicals reactive to DNA, e.g., the hydroxyl radical (·OH), leading to DNA-damage (Wardman et al 2008, Cadet *et al* 2017). Based on this evidence, as shown in the bottom right of Fig.1(B), in our previous modelling of the oxygen effects for DNA-targeted effects, the OER for early DNA double-strand breaks (DSBs) yield was incorporated as the ratio of the yield of potentially lethal lesions (PLLs) under oxygen rich condition ($p_{O_2} \geq 20\%$) to that under any oxygen pressure, p_{O_2} (%). The yield of PLL k (Gy^{-1}) is defined in the IMK model (Matsuya *et al* 2019). Calculating the ratio of k values under oxygen rich condition and any oxygen pressure, the OER can be expressed by

$$\mathrm{OER}(p_{O_2}) = \frac{k\,(\geq 20\%)}{k\,(p_{O_2})}, \quad [\therefore \mathrm{OER}\,(p_{O_2}) \geq 1.0] \tag{1}$$

where $k(p_{O_2})$ is the PLL yield under any oxygen pressure and $k(\geq 20\%)$ is the yield under oxygen rich condition. In this model, the oxygen rich condition (normoxia) was set as a fixed point because *in vitro* experiments in air can be easily performed. The coefficients for dose (D) and dose square (D^2) (i.e., α_0 and β_0) in the IMK model for DNA-targeted effects are proportional to OER and OER squared, respectively (Matsuya *et al* 2020a).

For intercellular signalling, we previously modelled the probabilities of a given cell having an activated target for emitting cell-killing signals and that of a cell having no activated targets based on microdosimetry, and expressed as the mean number of lethal lesions (LLs) per cell. To consider the oxygen dependence, based on the previous experimental data (Thompson *et al* 2017, Matsuya *et al* 2021), we now make the following assumptions:

(i) The mean number of targets activated for releasing intercellular signals per hit cell depends on oxygen pressure. The coefficients for D and D^2 for intercellular signals, α_b and β_b, are proportional to OER and OER squared, respectively, as shown in the bottom left of Fig. 1(B).

(ii) The OER value for DNA-targeted effects (i.e., ratio of early DSB yields) is applied to the model for intercellular signalling, which means that the probability of target activation for releasing cell-killing signals decreases in hypoxia.

(iii) The parameter representing the LL yield in non-hit cells δ (Matsuya *et al* 2018) is

independent of oxygen pressure, which indicates that the maximum number of LLs induced by intercellular signals per cell is constant.

Based on these assumptions for intercellular signalling, we modelled the in-field and out-of-field radiosensitivities in the same manner as the previous modelling.

2-2. *Surviving fraction of in-field and out-of-field cells*

Using the above assumptions, we modelled the surviving fractions of in-field and out-of-field cells based on the IMK model, which was previously developed for half-field exposures (Matsuya *et al* 2019). The present IMK model is composed of two parts, DNA-targeted effects and intercellular signalling (so called non-targeted effects).

We used the IMK model for DNA-targeted effects considering microdosimetry, sub-lethal damage repair (SLDR) during irradiation and oxygen effects, which has already been verified compared to the experimental data (Matsuya *et al* 2018 2019 2020a). The cell surviving fraction for DNA-targeted effects S_T can be given by

$$\begin{aligned} -\ln S_T = w_T &= \left(\alpha_0^* + \gamma_* \beta_0^*\right)\dot{D}T + \frac{2\beta_0^*}{(a+c)^2 T^2}\left[(a+c)T + e^{-(a+c)T} - 1\right]\left(\dot{D}T\right)^2 \\ &= \left(\alpha_0^* + \gamma_* \beta_0^*\right)D + F\beta_0^* D^2 \end{aligned} \tag{2}$$

where w_T is the number of LLs (residual lesions) per cell for DNA-targeted effects, $\dot{D}$ is constant dose-rate in Gy/h; T is dose-delivery time in hour; $(a+c)$ is the sum of the constant rate for a PLL to transform into a LL and that for DNA repair; γ_* is the microdosimetric quantity ($= y_D/\rho\pi r_d^2$) (the symbol * stands for either in-field (IF) or out-of-field (OF)); y_D is the dose-mean lineal energy in keV/μm (ICRU 1983), r_d and ρ are the radius and density of the microdosimetric site (so called domain), respectively (r_d = 0.5 μm, ρ = 1.0 g/cm^3) (Hawkins 1996). It should be noted that F describes the dose-rate effects induced by cell recovery during irradiation, which corresponds to the Lea-Catcheside time factor (Brenner 2008). The cell-specific parameters α_0^* and β_0^* are the coefficients to D (Gy^{-1}) and D^2 (Gy^{-2}). These coefficients depend on radiation field type even in case of the same cell line because of protective effects (intercellular communication). In our previous modelling, the protective effects were simply considered using the ratio of PLL yield under certain field type and uniform-field exposures, $\varphi_{PE} = k_{some}/k_{uniform}$ (Matsuya *et al* 2019), where k_{some} is the PLL yield for certain field-type exposure and $k_{uniform}$ is the yield for uniform-field exposure. Considering the oxygen effects OER(p_{O_2}) and the yield modification by radiation field type φ_{PE}, α_0^* and β_0^* are expressed by

$$\alpha_0^* = \frac{\alpha_0 \varphi_{PE}}{\mathrm{OER}(p_{O_2})} \quad \text{and} \quad \beta_0^* = \frac{\beta_0 \varphi_{PE}^2}{\mathrm{OER}(p_{O_2})^2} \tag{3}$$

where α_0 and β_0 were the coefficients for uniform-field exposure in normoxia. These coefficients were newly defined based on previous models of oxygen effects and the protective effects induced under modulated field exposure. In addition, the correction factor to consider the protective effects,

φ_{PE}, is newly defined in this modelling. This consideration of the OER value into the coefficients to dose and dose square can be linked to the previous modelling for oxygen effects based on the Linear-Quadratic (LQ) model (Carlson *et al* 2006).

The surviving fraction for intercellular signalling is modelled based on the previous modelling, which has been also verified compared to the experimental data (Matsuya *et al* 2019). In the same manner as DNA-targeted effects, OER(p_{O_2}) was incorporated into the model for intercellular signalling. The surviving fraction for intercellular signalling is expressed by

$$-\ln S_{IS} = w_{IS} = \delta\left[1 - e^{-(\alpha_b^* + \gamma_{IF}\beta_b^*)D_{IF} - \beta_b^* D_{IF}^2}\right] e^{-(\alpha_b^* + \gamma_* \beta_b^*)D_* - \beta_b D_*^2} \quad (4)$$

where S_{IS} is the surviving fraction for intercellular signalling (IS); α_b^* and β_b^* are cell-specific coefficients to D_* and D_*^2, respectively (* stands for either in-field (IF) or out-of-field (OF)); δ is the yield of lethal lesions (LLs) in non-hit cells. In the same manner as DNA-targeted effects, the coefficients (α_b^* and β_b^*) includes OER(p_{O_2}) defined in Eq. (1), which are expressed by

$$\alpha_b^* = \frac{\alpha_b}{\mathrm{OER}(p_{O_2})} \quad \text{and} \quad \beta_b^* = \frac{\beta_b}{\mathrm{OER}(p_{O_2})^2}. \quad (5)$$

Assuming that the interaction probability between sub-lesions (PLLs) induced by DNA targeted effects and intercellular signalling is very small (Sato *et al* 2014, Matsuya *et al* 2018), overall surviving fraction S can be expressed by

$$S = S_T \times S_{IS}. \quad (6)$$

The cell-specific parameters (α_0, β_0, $(a+c)$, α_b, β_b, δ, φ_{PE}) can be obtained from applying the model to the dose-response curve of cell survival in normoxia. γ can be determined from Monte Carlo simulation for radiation transport. OER can be obtained from ratio of DSB yields in normoxia and hypoxia or applying the model to the experimental survival data. Using Eqs. (1-6), we investigated the scenario of intercellular signalling in hypoxia.

3. Materials and Methods

3-1. Cell culture

To verify the developed model, we used two cancer cell lines, human prostate cancer (DU145) (RIKEN Science Institute BRC: Ibaraki, Japan), and non-small cell lung cancer (H1299) (ATCC: Manassas, VA, USA). DU145 cells were cultured in RPMI-1640 medium (Thermo Fisher Scientific Inc. Tokyo, Japan) with 10% fetal bovine serum (FBS, Nichirei Bioscience Inc., Tokyo, Japan) and 1% penicillin/streptomycin (p/s). H1299 cells were cultured in Dulbecco's Modified Eagle Medium (DMEM, Sigma-Aldrich Co., St. Louis, MO, USA) supplemented with 10% FBS and 1% p/s. Both DU145 and H1299 cells were maintained at 37 °C in a humidified atmosphere of 95% air/5% CO_2.

3-2. Hypoxic treatment

A nBIONIX-2 hypoxic cell culture kit (Sugiyamagen: Tokyo, Japan) (Kaida *et al* 2012) was used to induce hypoxic conditions *in vitro*. A cell culture dish containing the cultured cells and an AnaeroPack (oxygen absorber; Mitsubishi Gas Chemical, Tokyo, Japan) were placed inside a gas barrier pouch bag (Mitsubishi GasChemical) 4 h prior to irradiation. After placement, the oxygen concentration inside the pouch bag was continuously monitored until the sensitivity threshold of the OXY-2 oxygen monitor (JIKCO, Tokyo, Japan), which was 0.0% O_2. The radiobiological level of hypoxia was < 0.4% O_2 (McKeown *et al* 2014). After this hypoxic treatment, the cells were irradiated. After irradiation, the flasks were returned to normoxia.

3-3. Irradiation

Cells were irradiated with 150 kVp X-rays (1 mm Al filtration and 1.82 Gy/min) generated from an X-ray generator (MBR-1520R, Hitachi Medical Co., Tokyo, Japan). By shielding 50% area of a cell culture container, the dose was delivered to either 50% of the area of a culture container (so called half-field exposure) or 100% of the container (so called uniform-field exposure). As shown in the bottom of Fig. 1A, the dose profile in the half-field exposure was evaluated by the Monte Carlo simulation and the measurement with Gafchromic film as reported previously (Matsuya *et al* 2021), in which the out-of-field dose 1.0 cm away from dose boundary between in-field area and out-of-field one is 2.3% of the in-field doses.

3-4. Detection of residual DSB sites

The irradiated cells were fixed in 4% paraformaldehyde for 10 min on ice 24 h after irradiation. The fixed cells were permeabilized using 0.2% v/v Triton X-100 in phosphate buffered saline (PBS) for 5 min. The cells were then blocked in 1% bovine serum albumin (BSA) in PBS for 1 h. The cells were then incubated at 4°C overnight with primary antibodies against γ-H2AX (ab26350, Abcam) diluted 1:400 by the 1% BSA in PBS. After rinsing with 1% BSA in PBS three times, the cells were incubated in the dark at room temperature for 2 h with secondary antibodies Alexa Fluor 594-conjugated goat-anti-mouse IgG H&L (ab150116, Abcam) diluted 1:250 by a 1% BSA in PBS. After rinsing with the 1% BSA in PBS three times, the cells were incubated in the dark with 1 μg/ml DAPI solution (62248, Thermo Fisher Scientific) for 15 min. After rinsing once with methanol, we observed γ-H2AX foci using a Keyence BZ-9000 fluorescent microscope (Keyence, Osaka, Japan). The nuclear foci were evaluated with the automated foci counting module for peak detection using ImageJ software (Rasband *et al* 1997–2007, Abramoff *et al* 2004). The radiation-induced number of foci was further calculated by the subtraction of the number of background foci in non-exposed cells. The experiments were repeated four times and the standard error of the mean (s.e.m) was obtained.

3-5. Analysis of cell survival data

Using the experimental cell survival data for acute irradiation reported previously (Thompson *et al* 2017, Matsuya *et al* 2019 2021), we obtained a set of model parameters (α_0, β_0,

(a+c), γ, α_b, β_b, δ, φ_{PE}) for several cell models including DU145 prostate cancer cells, and H1299 and H460 lung cells. Note that the experimental survival data of H460 was used to check that the model works irrespective of the cell line type and hypoxic system that generated the experimental data. When determining the parameters, we used two Monte Carlo simulations: one is a track-structure simulation for determining microdosimetric quantity γ and the other is the Markov chain Monte Carlo (MCMC) simulation (Gelman *et al* 2014, Matsuya *et al* 2017) for determining cell-specific parameters (α_0, β_0, (a+c), α_b, β_b, δ) including the uncertainties. The procedures are described below.

First, the φ_{PE} values for DU145 and H1299 were obtained from the number ratio of the visible γ-H2AX foci 30 min after irradiation (i.e., the number ratio of foci under certain field type and that under uniform field) (Matsuya *et al* 2019). Second, the in-field and out-of-field microdosimetric qualities of γ in Gy was calculated by the radiation track-structure simulation with Particle and Heavy Ion Transport code system (PHITS) version 3.27 for X-rays (Sato *et al* 2018a) and WLTrack code for secondary electrons (Date *et al* 2007). The simulation accuracy for microdosimetry calculation was verified in our previous simulation (Matsuya *et al* 2019). Third, the in-field and out-of-field γ values and cell surviving fraction for half-field exposure (due to the largest number of experimental data) were used to determine the parameter set of (α_0, β_0, (a+c), α_b, β_b, δ) by the MCMC simulation. In this procedure, the φ_{PE} value for H460 cell line was simultaneously determined from the MCMC simulation due to no experimental γ-H2AX focus data being available. In the MCMC simulation, the uncertainty for –ln S was assumed to follow a normal distribution. The prior distributions (mean and standard deviation of the IMK model parameter) of DU145 cell line, which is necessary for the MCMC simulation, were obtained from our previous study (Matsuya *et al* 2019), and the parameters were updated by fitting to the cell survival data using MCMC. Similarly, for H1299 and H460, the previously determined distributions of the coefficients to doses for DNA-targeted effects (α_0, β_0) based on the Linear-Quadratic (LQ) model (Matsuya *et al* 2021) were used to efficiently determine the parameter set. The prior distributions of (a+c) for lung cancer cells were assumed to be normally distributed as 2.218 ± 0.401 (Matsuya *et al* 2017). Note that the (a+c) value depends on cell-cycle distribution (Matsuya *et al* 2020a). The other parameters were assumed to follow a uniform distribution due to no prior information.

Using the determined model parameters, we estimated the dose response of the surviving fraction after acute irradiation based on Eqs. (1-6). The OER(p_{O_2}) values defined in Eq. (1) were obtained from the OER for the DSB detected at 30 min after irradiation of 1 Gy (Matsuya *et al* 2021). As no experimental DSB data was available for the H460 cell line, the OER value for the survival endpoint (Thompson *et al* 2017) was used for the model prediction. The number of LLs (residual lethal lesions) per cell was also estimated by the IMK model (Eqs. (1-6)). The estimated dose responses of surviving fraction and nuclear LLs were compared to the corresponding experimental data measured in this study and the previous study (Thompson *et al* 2017, Matsuya *et al* 2021).

3-6. Statistical analysis

To evaluate the fit quality of the developed model, we calculated the coefficient of determination R^2 as statistical measures. The R^2 value used in this study is given by

$$R^2 = 1 - \frac{\sum_{i=1}^{n} (\exp_i - \mathrm{cal}_i)^2}{\sum_{i=1}^{n} (\exp_i - \langle \exp \rangle)^2}, \tag{7}$$

where $\exp_i$ is the measured data of surviving fraction or nuclear LLs per cell, cal_i is the estimation by the model, and <exp> is the mean experimental value. Note that log-transformed values were used when evaluating the fit quality for cell survival.

4. Results and Discussions

4-1. Estimation of cell survival in hypoxia

The IMK model considering oxygen effects for the half-field exposure was applied to the experimental dose-response curves for the survival of DU145, H1299 and H460 cells in normoxia. The model parameters were determined and are summarized in Table 1. Using the model parameters listed in Table 1, we estimated the dose response for in-field and out-of-field cells.

Figure 2 compares the survival curves between the prediction by the IMK model and the experimental data of DU145, H1299 and H460 (Thompson *et al* 2017, Matsuya *et al* 2021), in which (A) is the curves after the uniform-field (UF) cells, (B) is those of in-field (IF) cells after the half-field exposure, and (C) is those of out-of-field (OF) cells after the half-field exposure. The dose-mean lineal energy y_D values calculated by the Monte Carlo codes were summarized in Table 2, from which the γ values for in-field and out-of-field are 0.946 and 0.950, respectively. The higher y_D value of out-of-field compared to in-field value is attributed to the scattered X-rays from shielding materials (i.e., Pb). In Fig. 2, we compared the model prediction to the experimental survival of H460 cells to check that the model works irrespective of the experimental conditions (such as cell line type and hypoxic system) that generated the experimental data. As shown by the blue lines in Fig. 2, the dose response curves of in-field and out-of-field cells in normoxia can be reproduced by Eqs. (2), (4) and (6). The out-of-field responses were successfully reproduced by three cell-specific parameters (α_b, β_b, δ). Meanwhile, when estimating the surviving fraction of in-field cells uniformly exposed, we used the cell-specific coefficients (α_0, β_0) considering the change of PLL yields between half field and uniform field by the protective effects (Matsuya *et al* 2019), that were φ_{PE} = 0.936 ± 0.084 for DU145 cells, 0.941 ± 0.125 for H1299 cells, 0.944 ± 0.236 for H460 cells (see Table 1). Comparisons of the in-field dose response between the different field types (i.e., uniform field and half field) are described in Fig. S1 (see supplementary material) in which the reduced radiosensitivity of in-field cells after the half-field exposure was successfully reproduced by the IMK model.

Using the OER value and cell-specific parameters (α_0, β_0, $(a+c)$, α_b, β_b, δ), the in- and out-

of-field cell survival curves in hypoxia were predicted and are shown as the red lines in Fig. 2. To estimate surviving fraction in Fig. 2, we used two OER values. One is 2.31 obtained from the γ-H2AX foci data, and the other is 1.32 calculated from the ratio of doses during hypoxia compared to normoxia leading to 10% survival because the experimental initial DSB yields for H460 was not available. As these hypoxic conditions were created by either nBIONIX-2 or gas-exchanging system, the OER value is different each other. For the irradiation condition using the gas-exchange approach, we irradiated the DU145 cells in air after treatment in the nBIONIX-2 system. When the cells were exposed to oxygen during irradiation, the impact of hypoxia on radiosensitivity was reduced (see Fig. S2 in supplementary materials). These findings are similar to those in a previous report (Thompson *et al* 2017). However, both deliver sufficient hypoxia from radiobiological standpoint (McKeown *et al* 2014). The agreement between the IMK model predictions and the experimental survival curves under hypoxia (R^2 values for DU145, H1299 and H460 were 0.997, 0.994, 0.988, respectively, see Fig. 2) suggests that the model assumption that the hit probability for releasing cell-killing signals (i.e., intercellular signals) depends on oxygen concentration is reasonable. The same OER values were used for the uniform-field and half-field exposure in this study. In this regard, the model analysis suggested that the conventional OER value determined using uniform-field exposures can be applied when predicting both in- and out-of-field radiosensitivity of cells following exposure to intensity modulated beams.

To further verify the model for predicting out-of-field cell death, we also compared the model prediction with the experimental survival after at 8 Gy without intercellular signalling (IS). Figure 3 shows the comparison between the prediction by the IMK model with and without IS and the corresponding experimental data of DU145, H1299 and H460 at two conditions with OER = 1.32 and 2.31 (Thompson *et al* 2017, Matsuya *et al* 2021). We assumed that $\delta = 0$ when estimating the surviving fraction without IS, based on our previous model study (Matsuya *et al* 2019). From Table 2, the microdosimetric quantities represented as γ for in-field and out-of-field by 225 kVp X-rays were 0.895 and 0.972, respectively. In Fig. 3, the experimental out-of-field survival without intercellular signalling (IS) were measured by administrating 100 μM aminoguanidine, which is an inhibitor for inducible nitric oxide synthase (iNOS) (Matsuya *et al* 2021), or by irradiating with physical inhibition of cell-to-cell communication (in other word, 100% out-of-field cells) (Thompson *et al* 2017). As a result, with good agreement between the estimation and the experiment, the clonogenicities of out-of-field cells without IS were higher than those with the IS. iNOS down-regulates nitric oxide (NO). Therefore, the results suggested that cell-to-cell communication is significant and nitric oxide (NO) is dominant species for out-of-field cell killing even under hypoxia.

To date, the enhanced radiosensitivity of out-of-field cells (i.e., cell death and DNA lesions) in hypoxia can be attributed to bystander responses (Matsuya *et al* 2022). NO is a dominant factor leading to by cell death of bystander cells (Fig. 3) and can be regulated by the NF-κB pathway (which relates to inflammation) (Calveley *et al* 2005, Hamada *et al* 2011, Hei *et al* 2011). Taking account of these signalling pathways, inflammatory signalling may play a key role in out-of-field

radiosensitivity. Meanwhile, the reduction of radiosensitivity of in-field cells can be interpreted as protective effects by a reduction of early DNA damage (Matsuya *et al* 2019 2022) or rescue effects by stimulated DNA repair (Volcic *et al* 2012, Li *et al* 2019, Pathikonda *et al* 2020). The underlying mechanisms for the protective effects (as well as rescue effects) are still under investigation (Yu *et al* 2022), so further *in vitro* and *in vivo* studies are needed in future. Focusing on the impact of hypoxia, the radiosensitivities of out-of-field cells in hypoxia were found to be reduced compared to normoxia but dependent on the in-field absorbed dose (Thompson *et al* 2017, Matsuya *et al* 2021).

We also investigated the relationship between cell survival under normoxia and that under hypoxia using the IMK model, as shown in Fig. S3 (see supplementary material). The relationship estimated by the IMK model showed that hypoxia has only a small impact on out-of-field cells when in-field cells are exposed to a high dose. From these model predictions for cell survival, it is suggested that the role of the intercellular signalling (inflammatory responses) under hypoxia is similar to that in normoxia. From the model analysis, the differences between hypoxia and normoxia is interpreted to be due to the reduced probability for releasing cell-killing signals.

4-2. Application of the IMK model to residual DSBs

Radiation-induced cell killing is related to DSB induction. To further verify the developed model, we applied the model to experimental measurements of residual DSBs (LLs) after irradiation. In this study, we used the γ-H2AX foci formation assay to measure residual DSBs. Using the model parameters listed in Table 1, we then estimated the dose-response curves for in-field and out-of-field LLs per cell, and compared them to the experimentally determined nuclear γ-H2AX foci measured 24 h after irradiation.

Figure 4 compares the residual DSBs estimated by the IMK model and the experimental data obtained in this study where (AI) and (AII) are the curves in normoxia and (BI) and (BII) are those in hypoxia. The solid line and symbol are the estimation by the IMK model and the experimental data, respectively. The distribution of nuclear residual foci per cell are shown in Fig. S4 (see supplementary material), where increases for the unrepaired DNA lesions can observed in normoxia. This experimental distribution shown in Fig. S4 may be valuable for the future theoretical analysis considering cell-cycle distribution (Mori *et al* 2018). From these comparisons, the reductions of the residual DSB induction for both in-field and out-of-field cells were reproduced by the IMK model with good agreement. In particular, the dose responses for in-field cells followed a linear-quadratic response, while those of out-of-field cells exhibit a sigmoidal response as a function of in-field dose, which represents the hit probability for releasing cell-killing signals defined in the model assumption (see Fig. 1B).

As shown in Fig. 4, the residual DSBs can be related to the cell-killing induction with a certain probability (Carante *et al* 2015). In this regard, we also depicted the relationship between the residual nuclear DSBs 24 h after irradiation and the corresponding surviving fraction, which was shown in Fig. 5. Figures 5(A) and 5(B) show the relationship for in-field cells and out-of-

field cells, respectively. These results suggest that the correlation coefficient for out-of-field cells was lower than that for in-field cells (i.e., R^2 for out-of-field cells and in-field cells are 0.685 and 0.953, respectively), which is due to the experimental uncertainty. The model prediction for this relationship in Fig. 5(C) was derived based on the assumption that the number of LLs per nucleus follows a Poisson distribution (i.e., $-\ln S = w = w_T + w_{IS}$), which agreed well with the experimental relationship considering the experimental uncertainties ($R^2 = 0.965$). This tendency is the same as that obtained in previous efforts for interpreting the relationship between residual lesions and surviving fraction (Menegakis *et al* 2009, Olive *et al* 2011). In particular, in this study, it was found that the relationship of $-\ln S = w$ can be applied to, not only the conventional in-field responses, but also the out-of-field responses. In general, the phosphorylation expression of H2AX appears to be higher than the actual unrepaired DSBs, meaning the focus intensity does not correspond one-to-one to DSB (Rothkamm *et al* 2009). One limitation of this study is the use of single marker of DSB γ-H2AX, so the further experiments combined with 53BP1 is needed. Finally, considering the experimental limitations and the overall agreement with the experimental data (Figs. 2–5), the cellular mechanisms (i.e., oxygen-dependent hit probabilities inducing DNA targeted effects and intercellular communication) assumed in the presented model are reasonable, showing a good performance in reproducing biological impacts of in-field and out-of-field cells in hypoxia.

5. Conclusions

In this study, we modelled the cell-killing effects for intercellular communication under hypoxia. By using an oxygen enhancement ratio (OER) defined from DNA-targeted effects of early DSB yields (corresponding relative hit events), the present cell-killing model reproduced the experimental in- and out-of-field radiosensitivities considering intercellular signalling (i.e., the bystander effects on out-of-field effects and the protective effects on in-field cells). This model provides further interpretation of the role of intercellular communication in hypoxia showing that the yield of lethal DNA lesions in responding cells under hypoxia is lower than that in normoxia, and that the probability of hits for releasing cell-killing signals is dependent on oxygen. The modelling study indicates that the model analysis suggested that the conventional OER value determined using uniform-field exposure can be applied when predicting the in- and out-of-field radiosensitivity of cells following exposure to intensity modulated beams. These findings could contribute to a more precise understanding of intercellular signalling under heterogeneous exposure to intensity-modulated radiation fields.

The modelling of the radiobiological effects is a research topic of significant interest. Past models have been developed based on the experimental data *in vitro* with uniform radiation fields. However, from the recent experimental evidence, current estimation approaches based on the model parameters for uniform fields might be insufficient for predicting the responses to advanced radiotherapies using modulated beams. More advanced models for predicting curative effects of cancer-selective treatment such as boron neutron capture therapy (BNCT) and internal

409 radiotherapy with alpha emitters (Sato et al 2018b 2021, Matsuya *et al* 2020b) are also required.
410 Finally, to define the impacts on tumors as well as side effects on normal tissues (Sato *et al* 2022),
411 the accumulation of both experimental data *in vitro* and *in vivo* and modelling approaches is key
412 to future progress.
413
414 **CONFLICT OF INTEREST**
415 The authors declare that they have no conflict of interest.
416
417 **FUNDING**
418 This work was supported by the Japan Society for the Promotion of Science KAKENHI (Grant
419 no. 19K17215, 22H03744).
420
421 **SUPPLEMENTARY MATERIALS**
422 The following are available online:
423 ▪ Figure S1: Comparison of in-field cell survival between uniform field and half field
424 ▪ Figure S2: Radiosensitivity for various hypoxic cell culture systems
425 ▪ Figure S3: Relationship between cell survival under normoxia and that under hypoxia
426 ▪ Figure S4: Distribution of residual nuclear foci per cell
427
428 **AUTHOR CONTRIBUTIONS**
429 Y. Matsuya, S.J. McMahon and K.M. Prise designed this study. K.T. Butterworth provided the
430 experimental ideas using half-field exposure. Y. Matsuya, Y. Yachi and R. Saga performed the
431 cell experiments. Y. Matsuya and R. Saga developed the present IMK model. Y. Matsuya wrote
432 the manuscript. K.M. Prise and T. Sato supervised this study. All authors reviewed the manuscript.
433
434 **REFERENCES**
435 Abramoff MD, Magelhaes PJ, Ram SJ 2004 Image Processing with ImageJ *Biophot. Int.* **11**(7)
436 36–42
437 Bentzen SM 2009 Dose-response relationships in radiotherapy, In: Joiner M, van der Kogel AJ
438 (eds) Basic Clinical Radiobiology, London, Hodder Arnold 158–168
439 Brenner DJ 2008 The linear-quadratic model is an appropriate methodology for determining
440 isoeffective doses at large doses per fraction *Semin. Radiat. Oncol.* **18** 234–239
441 Butterworth KT, McGarry CK, Trainor C, O'Sullivan JM, Hounsell AR, Prise KM 2011 Out-of-
442 field cell survival following exposure to intensity modulated radiation fields *Int. J. Radiat.*
443 *Oncol. Biol. Phys.* **79**(5) 1516–1522
444 Cadet J, Davies KJ, Medeiros MH, Di Mascio P, Wagner JR 2017 Formation and repair of
445 oxidatively generated damage in cellular DNA *Free. Radic. Biol. Med.* **107** 13–34
446 Calveley VL, Khan MA, Yeung IW, Vandyk J, Hill RP 2005 Partial volume rat lung irradiation:
447 temporal fluctuations of infield and out-of-field DNA damage and inflammatory cytokines

following irradiation *Int. J. Radiat. Biol.* **81** 887–899

Carante MP, Altier S, Bortolussi S, Postuma I, Protti N, Ballarini F 2015 Modeling radiation-induced cell death: role of different levels of DNA damage clustering *Radiat. Environ. Biophys.* **54** 305–316

Carlson DJ, Stewart RD, Semenenko VA 2006 Effects of oxygen on intrinsic radiation sensitivity: A test of the relationship between aerobic and hypoxic linear-quadratic (LQ) model parameters *Med. Phys.* **33**(9) 3105–3115

Date H, Sutherland KL, Hasegawa H, Shimozuma M 2007 Ionization and excitation collision processes of electrons in liquid water *Nucl. Instr. Meth. B* **265**(2) 515–520

Gelman A, Carlin JB, Stern HS, Rubin DB 2014 Model Checking and Improvement, In: Gelman A, Carlin JB, Stern HS, Rubin DB Bayesian data analysis (vol.2) Boca Raton, FL, USA: Chapman & Hall/CRC 283–310

Ghita M, Coffey CB, Butterworth KT, McMahon SJ, Schettino G, Prise KM 2015 Impact of fractionation on out-of-field survival and DNA damage responses following exposure to intensity modulated radiation fields *Phys. Med. Biol.* **61**(2) 515–526

Gray LH, Conger AD, Ebert M, Hornsey S, Scott OC 1953 The concentration of oxygen dissolved in tissues at the time of irradiation as a factor in radiotherapy *Br. J. Radiol.* **26** 638–648

Hall EJ, Giaccia AJ 2006 Cell survival curves, In: Hall EJ, Giaccia AJ, Radiobiology for the Radiologist, 6th ed. Philadelphia: Lippincott Williams & Wilkins p. 31–46

Hall EJ, Giaccia AJ 2010 Oxygen Effect and Reoxygenation, In: Hall EJ, Giaccia AJ, Radiobiology for the Radiologist, 7th ed. Philadelphia: Lippincott Williams & Wilkins 96–103

Hamada N, Maeda M, Otsuka K, Tomita M 2011 Signaling Pathways Underpinning the Manifestations of Ionizing Radia-tion-Induced Bystander Effects *Curr. Mol. Pharmacol.* **4** 79–95

Hawkins RB 1996 A microdosimetric-kinetic model of cell death from exposure to ionizing radiation of any LET with experimental and clinical applications *Int. J. Radiat. Biol.* **69** 739–755

Hei TK, Zhou H, Chai Y, Ponnaiya B, Ivanov VN 2011 Radiation induced non-targeted response: mechanism and potential clinical implications *Curr. Mol. Pharmacol.* **4**(2), 96–105

ICRU 1983 Microdosimetry Report 36 *International Commission on Radiation Units and Measurements* Bethesda: MD

Kaida A, Miura M 2012 Differential dependence on oxygen tension during the maturation process betweenmonomeric Kusabira Orange 2 and monomeric Azami Green expressed in HeLa cells *Biochem. Biophys. Res. Commun.* **421** 855–859

Kuperman VY, Ventura AM, Sommerfeldt M 2008 Effect of radiation protraction in intensity-modulated radiation therapy with direct aperture optimization: a phantom study *Phys. Med. Biol.* **53** 3279–3292

Laurence VM, Ward R, Dennis IF, Bleehen NM 1995 Carbogen breathing with nicotinamide

improves the oxygen status of tumours in patients *Brit. J. Cancer* **72**(1) 198–205

Li D, Luo Y, Chen X, Zhang L-Y, Wang T, Zhuang Y, Fan Y, Xu J, Chen Y, Wu L 2019 NF-κB and Poly (ADP-ribose) Polymerase 1 Form a Positive Feedback Loop that Regulates DNA Repair in Acute Myeloid Leukemia Cells *Mol. Cancer Res.* **17**(3) 761–772

Matsuya Y, Kimura T, Date H 2017 Markov chain Monte Carlo analysis for the selection of a cell-killing model under high-dose-rate irradiation *Med. Phys.* **44**(10) 5522–5532

Matsuya Y, Sasaki K, Yoshii Y, Okuyama G, Date H 2018 Integrated Modelling of Cell Responses after Irradiation for DNA-Targeted Effects and Non-Targeted Effects *Sci. Rep.* **8** 4849

Matsuya Y, McMahon SJ, Ghita M, Yoshii Y, Sato T, Date H, Prise KM 2019 Intensity Modulated Radiation Fields Induce Protective Effects and Reduce Importance of Dose-Rate Effects *Sci. Rep.* **9** 9483

Matsuya Y, Sato T, Nakamura R, Naijo S, Date H 2020a A theoretical cell-killing model to evaluate oxygen enhancement ratios at DNA damage and cell survival endpoints in radiation therapy *Phys. Med. Biol.* **65**(9) 095006

Matsuya Y, Fukunaga H, Omura M, Date H 2020b A Model for Estimating Dose-Rate Effects on Cell-Killing of Human Melanoma after Boron Neutron Capture Therapy *Cells* **9**(5) 1117

Matsuya Y, McMahon SJ, Butterworth KT, Naijo S, Nara I, Yachi Y, Saga R, Ishikawa M, Sato T, Date H, Prise KM 2021 Oxygen enhancement ratios of cancer cells after exposure to intensity modulated x-ray fields: DNA damage and cell survival *Phys. Med. Biol.* **66** 075014

Matsuya Y, Hamada N, Yachi Y, Satou Y, Ishikawa M, Date H, Sato T 2022 Inflammatory signaling and DNA damage responses after chronic local exposure to a radioactive Cs-bearing microparticle *Cancers* **14** 1045

McGarry CK, Butterworth KT, Trainor C, O'Sullivan JM, Prise KM, Hounsell AR 2011 Temporal characterization and in vitro comparison of cell survival following the delivery of 3Dconformal, intensity-modulated radiation therapy (IMRT) and volumetric modulated arc therapy (VMAT) *Phys. Med. Biol.* **56** 2445–2457

McKeown SR, Cowen RL, Williams KJ 2007 Bioreductive drugs: from concept to clinic. *Clin. Oncol.* (*R. Coll. Radiol.*) **19**(6) 427-42

McKeown SR 2014 Defining normoxia, physoxia and hypoxia in tumours—implications for treatment response *Br. J. Radiol.* **87** 20130676

McMahon SJ, Butterworth KT, Trainor C, McGarry CK, O'Sullivan JM, Schettino G, Hounsell AR, Prise KM 2012 A Kinetic-Based Model of Radiation-Induced Intercellular Signalling *PloS One* **8** e54526

Menegakis A, Yaromina A, Eicheler W, Dörfler A, Beuthien-Baumann B, Thames HD, Baumann M, Krause M 2009 Prediction of clonogenic cell survival curves based on the number of residual DNA double strand breaks measured by γH2AX staining *Int. J. Radiat. Biol.* 85(11) 1032–1041

Monini C, Alphonse G, Rodriguez-Lafrasse C, Testa É, Beuve M 2019 Comparison of biophysical models with experimental data for three cell lines in response to irradiation with monoenergetic ions *Phys. Imag. Radiat. Oncol.* **12** 17–21

Mori R, Matsuya Y, Yoshii Y, Date H 2018 Estimation of the radiation-induced DNA double-strand breaks number considering cell cycle and absorbed dose per cell nucleus *J. Radiat. Res.* **59**(3) 253–260

Olive PL 2011 Retention of γH2AX foci as an indication of lethal DNA damage *Radiother. Oncol.* **101**(1) 18–23

Pathikonda S, Cheng SH, Yu KN 2020 Role of PARP1 regulation in radiation-induced rescue effect *J. Radiat. Res.* **61**(3) 352–367

Prise KM, O'Sullivan JM 2009 Radiation-induced bystander signalling in cancer therapy *Nature Reviews Cancer* 9 351–360

Rasband WS 1997–2007 ImageJ, U. S. National Institutes of Health, Bethesda, Maryland, USA, http://rsb.info.nih.gov/ij/

Rothkamm K, Horn S 2009 γ-H2AX as protein biomarker for radiation exposure *Ann. Ist. Super. Sanità.* **45**(3) 265–271

Sato T, Hamada N 2014 Model Assembly for Estimating Cell Surviving Fraction for Both Targeted and Nontargeted Effects Based on Microdosimetric Probability Densities *PLOS ONE* **9**(11) e11405

Sato T, Iwamoto Y, Hashimoto S, Ogawa T, Furuta T, Abe S, Kai T, Tsai PE, Matsuda N, Iwase H, Shigyo N, Sihver L, Niita K 2018a Features of Particle and Heavy Ion Transport code System (PHITS) version 3.02 *J. Nucl. Sci. Technol.* **55**(5-6), 684–690

Sato T, Masunaga S-I, Kumada H, Hamada N 2018b Microdosimetric Modeling of Biological Effectiveness for Boron Neutron Capture Therapy Considering Intra- and Intercellular Heterogeneity in ^{10}B Distribution *Sci. Rep*. **8** 988

Sato T, Hashimoto S, Inaniwa T, Takada T, Kumada H 2021 Implementation of simplified stochastic microdosimetric kinetic models into PHITS for application to radiation treatment planning *Int. J. Radiat. Biol.* **97**(10) 1450–1146

Sato T, Matsuya Y, Hamada N 2022 Microdosimetric modeling of relative biological effectiveness for skin reactions: Possible linkage between in vitro and in vivo data *Int. J. Radiat. Oncol*. 114(1) 153–162

Scholz M, Friedrich T, Magrin G, Colautti P, Ristić-Fira A, Petrović I 2020 Characterizing Radiation Effectiveness in Ion Beam Therapy Part I: Introduction and Biophysical Modeling of RBE Using the LEMIV *Front. Phys.* **8** 272

Sugano Y, Mizuta M, Takao S, Shirato H, Sutherland KL, Date H 2015 Optimization of the fractionated irradiation scheme considering physical doses to tumor and organ at risk based on dose–volume histograms *Med. Phys.* **42** 6203–6210

Thompson HF, Butterworth KT, McMahon SJ, Ghita M, Hounsell AR, Prise KM 2017 The Impact of Hypoxia on Out-of-Field Cell Survival after Exposure to Modulated Radiation

565 Fields *Radiat. Res.* **188**(6) 716–724
566 Trainor C, Butterworth KT, Mcgarry CK, Liberante F, Sullivan JMO, Hounsell AR, Sullivan O,
567 Prise KM 2012 Cell survival responses after exposure to modulated radiation fields *Radiat.*
568 *Res.* **51** 44–51
569 Volcic M, Karl S, Baumann B, Salles D, Daniel P, Fulda S, Wiesmüller S 2012 NF-κB regulates
570 DNA double-strand break repair in conjunction with BRCA1–CtIP complexes *Nucleic*
571 *Acids Res.* **40**(1) 181–195
572 Wardman P 2009 The importance of radiation chemistry to radiation and free radical biology (The
573 2008 Silvanus Thompson Memorial Lecture) *Br. J. Radiol.* **82** 89–104
574 Withers HR 1975 The four R's of radiotherapy *Adv. Radiat. Biol*. **5** 241–271
575 Yu KN 2022 Role of radiation-induced rescue effect in radiation field size effect *Radiat. Phys.*
576 *Chem.* **200** 110143.

Figure captions:

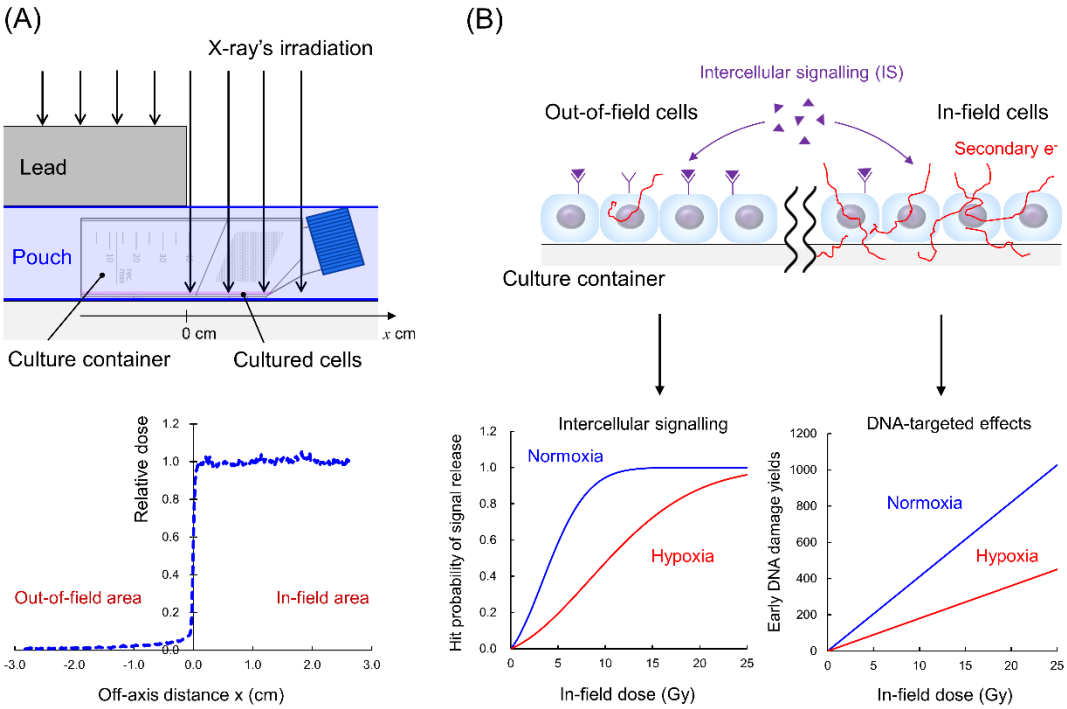

Figure 1. Schematic illustration of half-field exposure and the biological effects: (A) is the experimental geometry of the half-field exposure in which by shielding 50% of a cell culture flask was irradiated. The experimental dose profile is given in our previous report (Matsuya *et al* 2021). (B) is the model for oxygen effects for DNA-targeted effects and intercellular signalling. The oxygen dependence on early DNA lesion yields was incorporated into the modelling for the DNA-targeted effects, which has been developed previously (Matsuya *et al* 2020a), while the oxygen-dependent hit and non-hit probabilities for releasing cell-killing signals was newly considered in this IMK model.

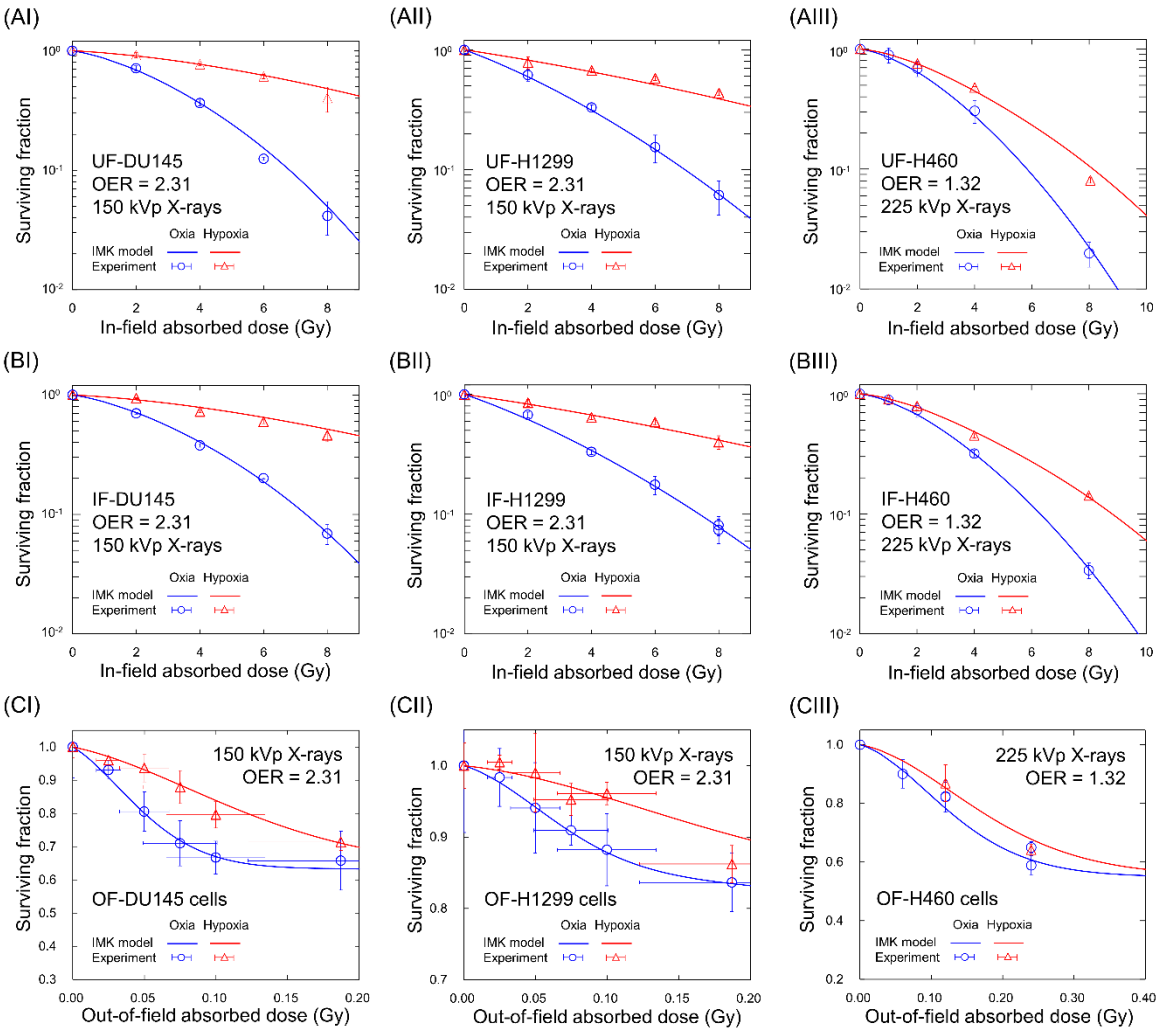

Figure 2. Dose-response curve of cell survival: (A) is the curves after uniform-field (UF) exposure, (B) is those of in-field (IF) cells after the half-field exposure, and (C) is those of out-of-field (OF) cells after the half-field exposure. The left panels are the curves of DU145, the central those are H1299 and the right those are H460. The line and the symbol represent the prediction by the IMK model and the experimental data reported in our previous studies (Thompson *et al* 2017, Matsuya *et al* 2021), respectively. Note that the experimental surviving fractions were calculated by the ratio of plating efficiency of irradiated group to that of the non-irradiated group (control cells). The out-of-field dose for 225 kVp and 150 kVp X-rays are 3.00% and 1.25% of in-field dose, respectively. The in-field dose rates for 150 kVp X-rays and 225 kVp X-rays were 1.82 and 0.591 Gy/min, respectively. The R^2 values for DU145, H1299 and H460 were 0.997, 0.994, 0.988, respectively.

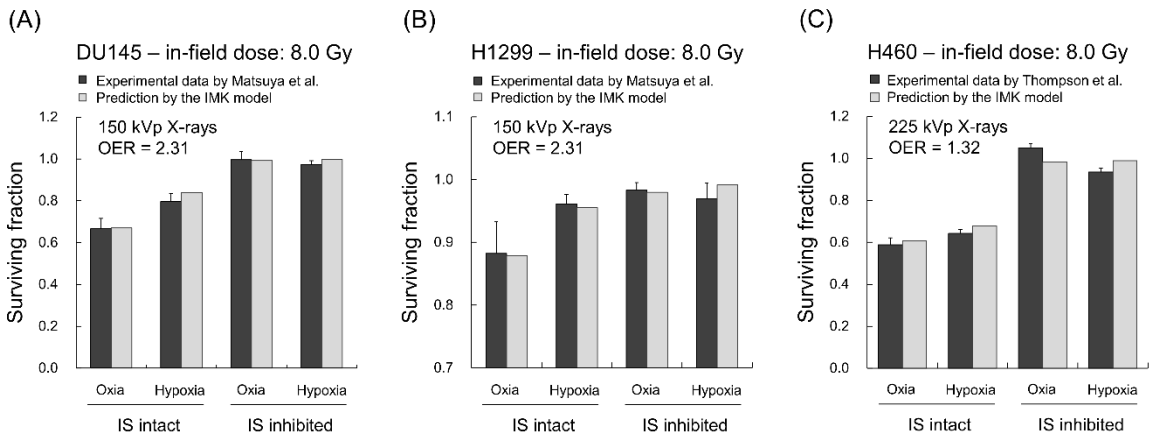

Figure 3. Out-of-field surviving fraction after 8 Gy irradiation with and without intercellular signals: (A) is the DU145 for OER = 2.31, (B) is the H1299 for OER = 2.31, (C) is the H460 for OER = 1.32. The IMK model agreed well with the experimental data (Thompson *et al* 2017, Matsuya *et al* 2021). We assumed that $\delta = 0$ when estimating the surviving fraction without IS, based on our previous model study (Matsuya *et al* 2019). The out-of-field dose for 225-kVp and 150-kVp X-rays are 3.00% and 1.25% of in-field dose, respectively. The in-field dose rates were 1.82 Gy/min for 150 kVp and 0.591 Gy/min for 225 kVp.

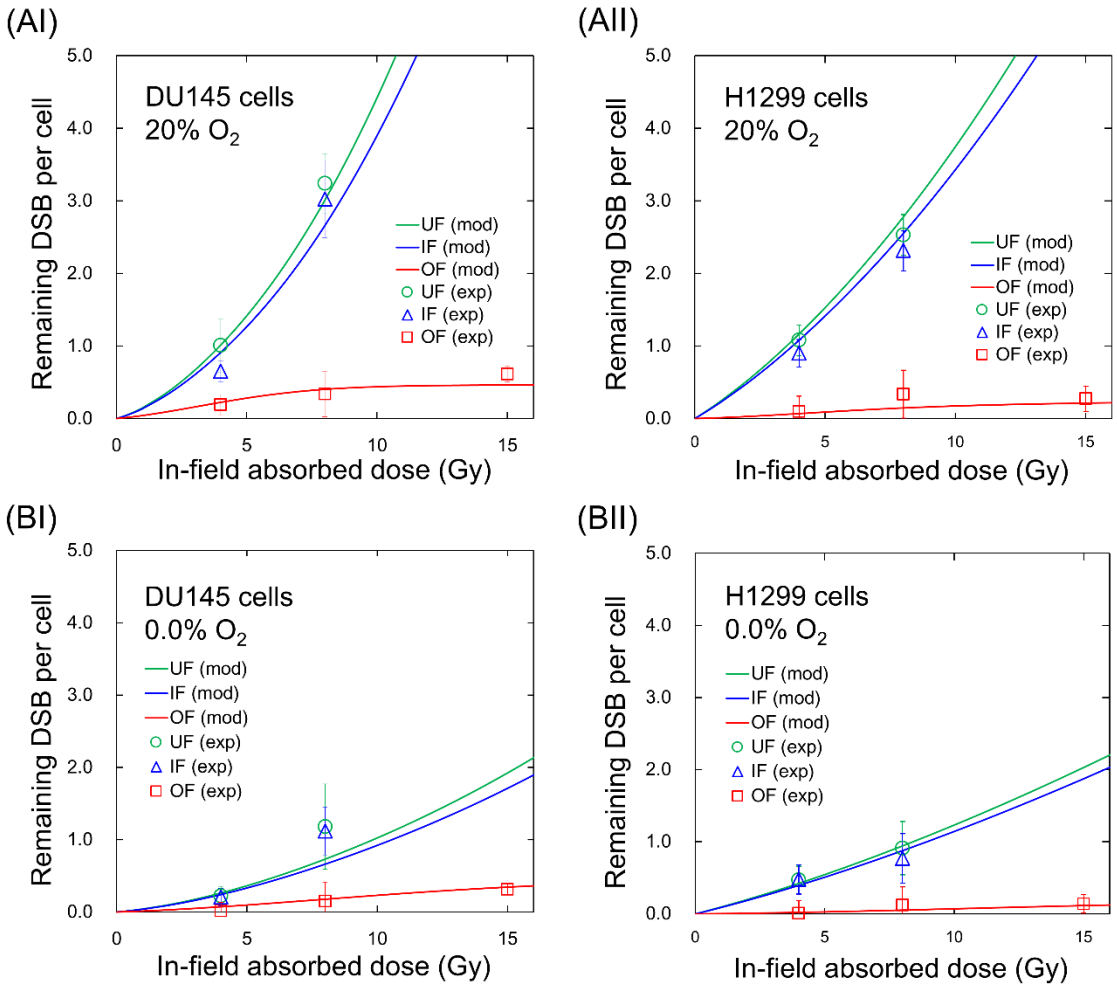

Figure 4. Residual DSBs 24 after irradiation: (AI) and (AII) are the curves in normoxia, and (BI) and (BII) are those in hypoxia. The left panels are the curves of prostate cancer cells DU145 and the right those are non-small cell lung cancer H1299. Solid line and symbol are the estimation by the IMK model (based on Eqs (1-6)) and the experimental data measured by the γ-H2AX focus formation assay. The out-of-field dose is 2.28% of in-field dose. In the same manner as Fig. 2, the in-field dose rate was 1.82 Gy/min. The R^2 values for DU145 and H1299 were 0.964 and 0.970, respectively.

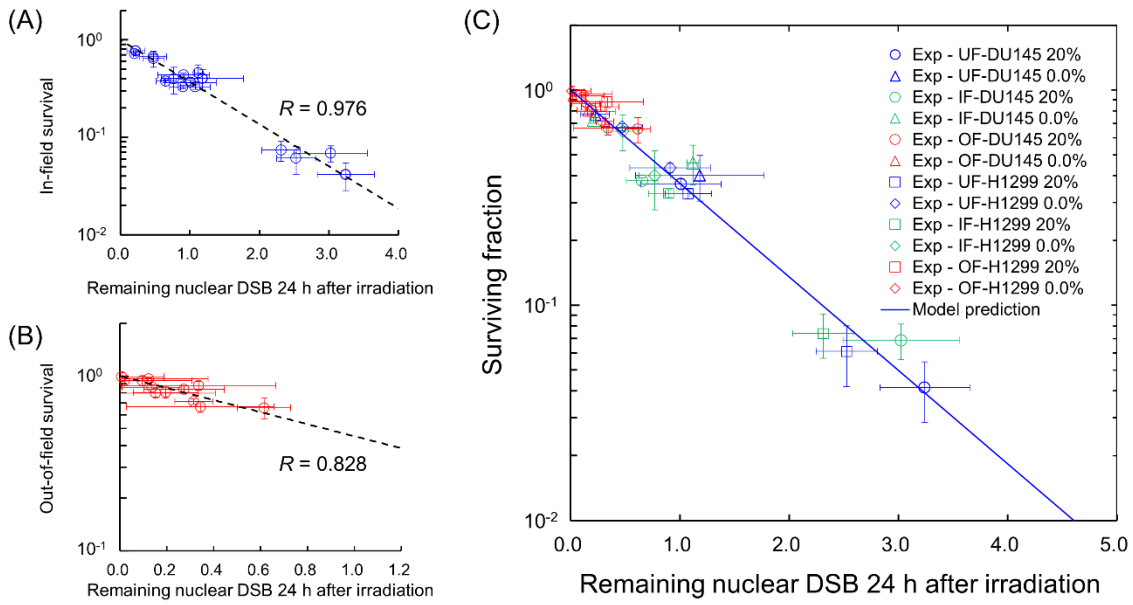

Figure 5. Relationship between the remaining nuclear DSB 24 h after irradiation and surviving fraction: Solid line and symbol are the estimation by the IMK model ($-\ln S = w = w_T + w_{IS}$) and the experimental data measured by the γ-H2AX focus formation assay. OF, IF and UF mean out-of-field for half-field exposure, in-field for half-field exposure and uniform-field exposure, respectively. This comparison between model prediction and the experimental data proves that the residual DSB can be linked to the cell-killing induction with a certain probability.

Table 1. Cell-specific model parameters in the IMK model for oxic condition

Effect type	Parameters	Cell line type			Unit
		DU145	H1299	H460	
DNA-targeted effects	α_0	0.035 ± 0.007	0.203 ± 0.027	0.020 ± 0.015	Gy^{-1}
	β_0	0.039 ± 0.005	0.017 ± 0.003	0.058 ± 0.007	Gy^{-2}
	$a+c$	2.092 ± 1.306	2.207 ± 0.401	2.222 ± 0.389	h^{-1}
Protective effects	φ_{PE} [a,b]	0.936 ± 0.084	0.941 ± 0.125	0.944 ± 0.236	-
Intercellular signalling	α_b	0.045 ± 0.024	0.017 ± 0.018	0.011 ± 0.037	Gy^{-1}
	β_b	0.025 ± 0.006	0.018 ± 0.007	0.025 ± 0.010	Gy^{-2}
	δ	0.450 ± 0.048	0.144 ± 0.025	0.571 ± 0.086	-

[a] These values for DU145 and H1299 were obtained from yield ratio of γ-H2AX foci (Matsuya *et al* 2021), while that for H460 was determined by the MCMC simulation.

[b] The φ_{PE} values presented in this table for half-field exposure. When obtaining α_0^* and β_0^* for the uniform field exposure, we set φ_{PE} to be 1.00.

Table 2. Microdosimetric quantities calculated by Monte Carlo simulations

Radiation type	Shielding block	Field type	Dose-mean lineal energy y_D [keV/μm]
150 kVp X-rays	2.1-cm thick Pb	In-field	4.643 ± 0.066
		Out-of-field	4.687 ± 0.086
225 kVp X-rays	5.0-cm thick Pb	In-field	4.393 ± 0.007 [a]
		Out-of-field	4.769 ± 0.044 [a]

[a] The values for 225 kVp X-rays were obtained from the previous report (Matsuya *et al* 2019).